

Oxidation of Aluminum Particles from 1 to 10 nm in Diameter: The Transition from Clusters to Nanoparticles

Kyle R. Overdeep,^{*,†,‡,§} Claron J. Ridge,^{†,‡} Yan Xin,[§] Tonya N. Jensen,^{||} Scott L. Anderson,^{||,§} and C. Michael Lindsay[‡]

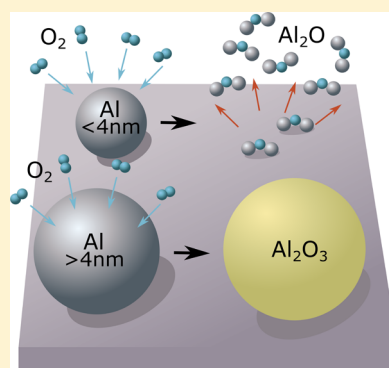
[†]Department of Nanochemistry & Nanoengineering, University of Dayton Research Institute, Dayton, Ohio 45469, United States

[‡]Energetic Materials Branch, Air Force Research Laboratory, Eglin Air Force Base, Florida 32542, United States

[§]National High Magnetic Field Laboratory, Florida State University, Tallahassee, Florida 32310, United States

^{||}Department of Chemistry, The University of Utah, Salt Lake City, Utah 84112, United States

ABSTRACT: Micrometer- and nanometer-scale aluminum (nAl) particles are often considered attractive choices for fuels in energetic materials. In general, reaction rates increase as particle size decreases because of the increased surface area and reduced diffusion lengths between reactants. The oxidation behavior for aluminum nanoparticles >10 nm in diameter has been widely studied, and so has the oxidation behavior of clusters <1 nm in diameter (primarily for catalysis applications). These two regimes exhibit vastly different reaction mechanisms, but there is no experimental work observing the oxidation behavior for intermediate size particles with diameters from 1 to 10 nm. The present study investigates this transition regime by producing unpassivated aluminum particles in this size range using superfluid helium droplet assembly (SHeDA) and then oxidizing the particles by rapidly transferring them from ultrahigh vacuum (UHV) to ambient air. Scanning transmission electron microscopy with energy dispersive spectroscopy (STEM/EDS) and X-ray photoelectron spectroscopy (XPS) showed that particles <4 nm in diameter vaporize upon oxidation while particles >4 nm in diameter do not. We have hypothesized that this is a critical diameter and is the threshold between the oxygen-etching mechanism of clusters and the heterogeneous oxidation of nanoparticles.



I. INTRODUCTION

Aluminum particles are an important material to study because of their utility in energetic materials.^{1–3} Their performance is inherently linked to particle size for many reasons,⁴ most notably because a smaller length scale allows for more intimate mixing with an oxidizer and increases the surface area to volume ratio, therefore potentially increasing the reaction rates. There is a large body of literature on the oxidation of micrometer and nanoscale aluminum down to tens of nanometers in diameter for energetics^{5–11} as well as aluminum atomic clusters up to ≈ 40 atoms for catalysis.^{12–21} There is a distinct lack of experimental work, however, on particles in the range between atomic clusters and conventional nanoparticles, with diameters from approximately 1 to 10 nm (20 to 30000 atoms).^a There are, however, some computational simulations for this size range.^{22–26}

The transition between clusters and nanoparticles is an interesting size range to study due to the disparity in oxidation behavior between clusters and nanoparticles, which implies that there is likely a transition in oxidation mechanism within this range. The reactions between aluminum clusters and oxygen are etching processes, and the products (e.g., Al_2O) are ejected as they form due to the rapid heat generation and weak binding energy to the rest of the cluster at such small diameters. The residual heat can cause the subsequent

evaporation of additional aluminum. An exact mechanism has been proposed for Al clusters in the gas phase²⁷ and seems to be similar for negatively charged, positively charged, and neutral clusters.^{15,18,19,28} It is unclear what the effect of energy transfer to a support is on the tendency toward evaporation. Reactions between free-standing aluminum nanoparticles (tens of nanometers in diameter) and oxygen, however, are thought to follow heterogeneous oxide growth²⁹ and/or the melt dispersion mechanism.³⁰ Neither mechanism would result in etching away the particle, though the melt dispersion mechanism does result in the spallation of small nanoparticles.

There also tend to be important experimental differences between studies involving clusters versus studies involving nanoparticles: cluster oxidation is typically performed under vacuum at room temperature with some controlled amount of oxygen bled into a reaction chamber downstream of the cluster source. The oxidation of condensed-phase aluminum clusters has never before been studied; few cluster studies are performed with clusters deposited onto substrates, and those that were exposed to air were chemically bonded to the substrate, altering the chemical makeup and therefore also

Received: June 11, 2019

Revised: August 30, 2019

Published: September 13, 2019

altering the oxidation behavior of the particles.^{31–35} Nanoparticle oxidation, however, is frequently performed under extreme conditions, at pressures up to 32 atm and temperatures of up to 3000 K after shock initiation.^{36,37} Additionally, most nanoparticles already have an oxide passivation layer, which gas-phase clusters created in vacuo lack. It is difficult to develop a cohesive view spanning all particle sizes when each regime is investigated under such disparate conditions. It is therefore our goal to create intermediate size particles from 1 to 10 nm in diameter and observe their oxidation behavior under intermediate conditions via oxidation in low partial pressures of oxygen in a vacuum up to ambient air. Other relevant studies performed with similar conditions are limited to the passivation of aluminum films as a function of time, temperature, and oxygen pressure in a vacuum.³⁸

The scarcity of data in the transition regime is largely due to the difficulties associated with fabricating nanoparticles in this size range, but it is possible by using superfluid helium droplet assembly (SHeDA), in which liquid helium droplets are doped with atoms to form particles. The helium droplets maintain a temperature of 0.4 K by evaporating helium atoms to dissipate any heat gained during the dopant pickup and aggregation process. This ultralow-temperature bath freezes out reactions that might occur within the incipient cluster, enabling the production of metastable structures, like core–shell particles, that are challenging or impossible to make by other methods.³⁹ The contents of the droplet can be measured in the gas phase using in-situ quadrupole mass spectroscopy or soft-deposited onto a substrate for ex-situ analysis.⁴⁰

In addition to various single-component particles, superfluid helium droplet assembly (SHeDA) has also been used to generate core–shell particles of various combinations including magnesium/copper,⁴⁰ magnesium/perfluoropolyether,⁴¹ and silver/gold.⁴² Although the instrument is unique, other groups do similar work with organics, metals, and various other dopant materials.^{39,42–46} By making aluminum particles with this method, we bridge the gap between aluminum clusters and conventional aluminum nanoparticles to understand how aluminum particles behave at their lower size limit.

II. EXPERIMENTAL SECTION

The full design and function of SHeDA have been described previously.⁴⁷ The schematic presented in Figure 1 provides an overview of the process. In short, 99.999% pure helium (supplied by Airgas) is forced through a cold nozzle with an aperture of 3.1 μm , and the helium condenses into liquid droplets as it isentropically expands into a vacuum. The combination of nozzle temperature (4.5–12 K) and helium pressure (15–100 bar) dictates the size of the helium droplets, ranging from 1×10^3 to 1×10^{10} atoms (4 nm–1 μm in diameter).⁴⁸ The droplets are skimmed to form a beam that passes over effusion cells containing the desired dopants, and the droplets intercept, incorporate, and cool the dopant atoms or molecules. Generally, the dopant material goes toward the center of the droplet where it condenses into a cluster. Several species have been identified that are most stable on the exterior of the helium droplet, including aluminum atoms in an excited state, but the ground-state aluminum atoms are expected to reside at the center of the droplet.⁴⁴ The cluster size is a function of how many dopant atoms or molecules the droplet intercepts and therefore depends upon droplet size, velocity, and the vapor density of the dopant. By varying these parameters, we can adjust the cluster size from 1 to 1×10^5

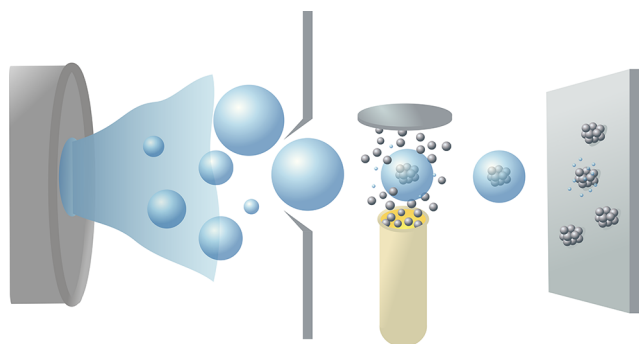


Figure 1. Schematic of superfluid helium droplet assembly (SHeDA), all under high vacuum. Pressurized helium is forced through a cold nozzle, and at the nozzle temperatures relevant to this work, the liquid helium breaks up into droplets that maintain a temperature of 0.37 K. The droplets intercept dopant aluminum atoms over an effusion cell. The droplets impact a substrate, evaporating helium, and the clusters soft-land on the substrate. This schematic is not to scale.

atoms (up to ≈ 20 nm in diameter), frequently with a wide size distribution. The transition size nanoparticles produced in this study (diameters from 1 to 10 nm) are produced by using high doping rates of large helium droplets. The helium droplets maintain a temperature of 0.37 K throughout the process by evaporating helium to dissipate energy gained from picking up hot dopants, and more significantly, the cohesive energy released when those dopants combine into particles.³⁹ The particles are deposited with a very low impact energy on the order of 0.05 eV/atom because the helium evaporates as it impacts the substrate, creating a vapor cushion.^{49,50}

The particle sizes were estimated by monitoring helium beam depletion, as observed by using quadrupole mass spectrometry (Extrel CMS, LLC, 1–500 amu). It has been shown that the reduction in helium cluster fragment flux upon electron ionization is proportional to the doping rate within the droplets, which allows the particle size to be calculated for the initial number of helium atoms per droplet.⁴⁸ The base vacuum pressure in the instrument was $\sim 6 \times 10^{-9}$ Torr. All samples were deposited for 1 h to obtain the desired substrate coverage such that there are enough clusters in a given area to attain statistical significance, but not so many particles that they would interact or agglomerate (roughly 100–1000 clusters/ μm^2). The helium beam passed directly between the lip of the cell and a shutter positioned 1 cm above the lip. The shutter caused the hot atoms to bounce back toward the oven and served to increase the vapor density in the beam and therefore also increase the doping rate. The effusion cell containing aluminum was held at ~ 1350 °C to achieve 50% helium beam depletion (for nozzle conditions of 9 K and 20 bar), which was found to be a good compromise in providing sufficient doping while still maintaining a large enough droplet for soft landing. Lower doping rates were used for samples produced in larger helium droplets, however, because 50% depletion was not attainable even with the aluminum effusion cell operating at the maximum temperature.

Clusters were deposited onto ultrathin amorphous carbon film transmission electron microscopy (TEM) grids (Ted Pella, Inc.) and 1 cm \times 1 cm silicon wafers (MTI) that were washed with acetone and methanol prior to use. The beam of helium droplets was ~ 1 cm in diameter at the substrate, and so it was possible to deposit onto both types of substrates simultaneously to remove any run-to-run variability. After

deposition, the samples were withdrawn into an exchange chamber, which was then vented to ambient air as quickly as possible after deposition. Particle interactions with the substrate were minimal, and oxidation behavior seemed to be consistent regardless of the substrate.

The samples on amorphous carbon were analyzed by annular dark-field scanning transmission electron microscopy (ADF-STEM) imaging and by energy dispersive spectroscopy (EDS). ADF-STEM was performed on a probe-aberration-corrected cold-field emission JEOL JEM-ARM200cF microscope at 200 kV, equipped with an EDAX EDS Si(Li) detector. The resulting images were analyzed to obtain average particle sizes and aspect ratio by using the Cornell Spectrum Imager plugin⁵¹ for Fiji.⁵² Reported diameters are the average of the minimum and maximum Feret diameters for roughly 40 particles from multiple representative images. The number of particles was limited because accurate calculations required high-magnification images with relatively few particles in each image, and particles touching others could not be used. The “unoxidized diameter” was estimated by calculating the number of aluminum atoms in an average size oxidized particle and backing out the diameter for a metallic particle with that number of atoms. The calculation used bulk values for molar volumes of aluminum and aluminum oxide. The EDS results were scaled such that the carbon peak intensities (0.3 keV) were 100 counts for each sample. This was found to be the most reliable way to compare all EDS results, since the underlying grid material is carbon with similar thicknesses, and so it was a relatively consistent background signal for each test. The peaks corresponding to aluminum (1.5 keV) were fit with Gaussian curves and integrated to determine their areas after proper background subtraction.

The samples on silicon were analyzed by using X-ray photoelectron spectroscopy (XPS) performed with a monochromatic Al K α (1486.6 eV) X-ray source on a Kratos Axis Ultra DLD instrument, with a $300 \times 700 \mu\text{m}^2$ spot size. A charge neutralizer was used to mitigate charging. The spectrum was fit by using CasaXPS. A Shirley algorithm was applied for the background, and peaks were fit with a Gaussian/Lorentzian-type function. The binding energy scale was adjusted so that the elemental silicon 2s peak from the silicon wafer substrate was centered on 151 eV.⁵³ This required no more than a 200 meV shift for any spectra, i.e., far less than the peak separations.

EDS and XPS spectra were also obtained for clean substrates (TEM grids and silicon wafers, respectively) that were placed in SHeDA and exposed to the helium beam *without* aluminum doping as “blank” runs. They both showed that there is no aluminum above the level of background noise, whether as a substrate impurity or instrumental contamination.

III. RESULTS

Quadrupole mass spectrometry was used to confirm that aluminum atoms were being incorporated into the helium droplets and were forming particles at the relevant beam conditions. Two mass spectra were recorded—one with aluminum doping and one without—and the difference spectrum (after smoothing with a Savitzky–Golay filter) is plotted in Figure 2. The positive peaks highlight what increased upon incorporation of the aluminum. Clusters up to Al_3^+ are shown as well as a small amount of Al_2O^+ that forms from the aluminum scavenging oxygen, likely from residual water vapor in the vacuum chamber. $\text{Al}_x\text{-He}_n^+$ “snowballs” are

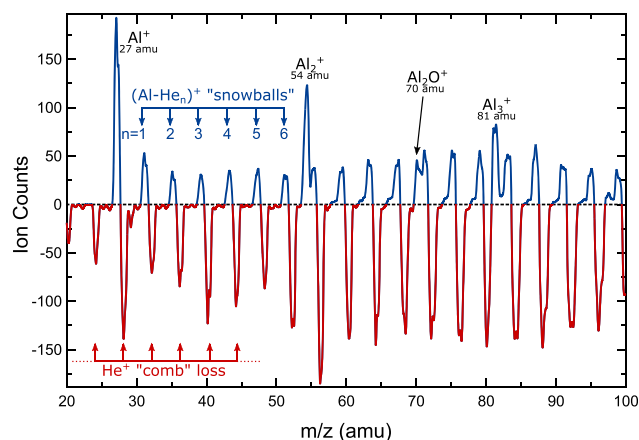


Figure 2. Mass spectrum of helium droplets *without* aluminum clusters subtracted from one *with* aluminum clusters. Positive peaks show the aluminum clusters in the helium beam, and negative peaks show the helium lost from incorporating aluminum. In this example, the average helium droplet size is $\sim 5 \times 10^5$ atoms, or 20 nm in diameter, formed at a nozzle temperature of 9 K and a helium pressure of 15 bar.

also seen as peaks that occur every 4 amu from helium atoms essentially sticking to the aluminum clusters during the ionization process and are commonly observed with non-molecular clusters.⁵⁴ The negative peaks show what was lost when aluminum was doped into the helium droplets. These peaks are referred to as the helium “comb” that results from helium boiling off to dissipate the heat from forming aluminum clusters.⁵⁵ The helium depletion was measured for each sample and served as a confirmation that aluminum was being incorporated into the helium beam at the expected rate.

Transition size nanoparticles were deposited for 1 h onto the TEM grids and then rapidly oxidized by removing the samples from UHV ($\approx 5 \times 10^{-8}$ Torr) and exposing them to ambient air (760 Torr) at $\approx 35\%$ relative humidity within ~ 1 s. The deposition parameters and the particle sizes measured by using ADF-STEM images are listed in Table 1. The micrograph in Figure 3a shows a blank substrate for sample 1, which the smallest particles (1.8 nm in diameter) were deposited onto. Figure 3b shows sample 2, the particles predicted to be an average diameter of 6.5 nm. Particles were present, though less numerous than anticipated based on calculations of surface coverage using nozzle throughput and skimmer efficiency for our beam conditions.⁴⁷ The average diameter was 8.2 ± 2 nm for the aluminum oxide product, corresponding to an unoxidized diameter of ≈ 7.5 nm, which is slightly larger than the predicted 6.5 nm. Sample 3, with a predicted particle diameter of 13.7 nm, is shown in Figure 3c. Unlike sample 2, the particle coverage was higher than predicted by a factor of 7 \times , and the average diameter of the aluminum oxide particles was smaller than anticipated, about 9.2 ± 4.8 nm, which correlates to an unoxidized diameter of about 8.4 nm. The observation of more numerous, smaller clusters than predicted indicates that multicenter growth occurred for this sample, which is a well-known phenomenon for large helium droplets and high doping rates where there is a high probability that the dopant atoms collide and form particles in multiple locations within the droplet.^{42,56} The average aspect ratio for particles in samples 2 and 3 were 1.8 and 2.0, respectively. These relatively high ratios are the result of the larger helium droplet sizes required for these samples based on a well-documented

Table 1. Sample Deposition Conditions and Calculated Substrate Coverage

sample	predicted mean particle size (atoms)	predicted mean particle diameter (nm)	measured mean particle diameter (nm)	nozzle temperature (K)	helium pressure (bar)	average droplet size (atoms)	predicted aluminum fluence (atoms/ μm^2)
1	1.7×10^2	1.8		9	20	1.8×10^6	4.1×10^7
2	8.6×10^3	6.5	7.5 ± 1.5	6	20	3.1×10^8	2.0×10^7
3	8.1×10^4	13.7	8.4 ± 4.5	9	100	$\approx 1 \times 10^{10}$	6.0×10^7

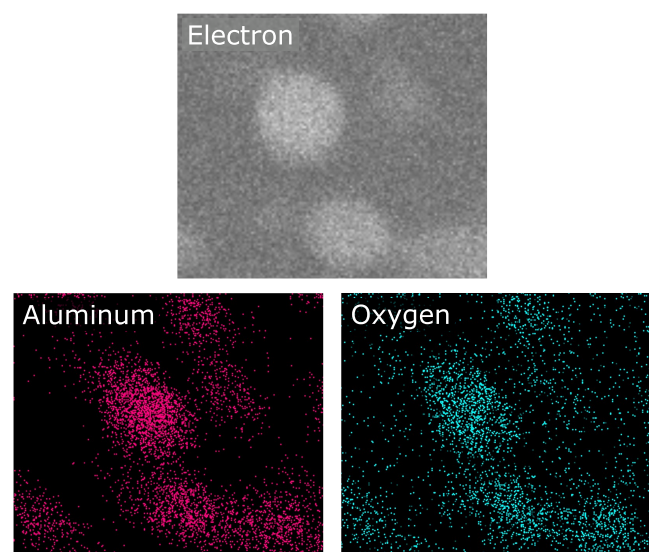


Figure 3. ADF-STEM images of substrates onto which aluminum transition size nanoparticles were deposited with average diameters of (a) 1.8, (b) 7.5, and (c) 8.4 nm and then exposed to ambient air. There are no particles <4 nm in diameter present after oxidation. (d) Energy dispersive spectroscopy (EDS) elemental maps from the 8.4 nm diameter particles showing that they are oxidized, as anticipated. These are representative of all particles present.

phenomenon of string formation in superfluid helium droplet assembly.^{57,58}

EDS spectra and elemental mapping of representative particles (from sample 3), shown in Figure 3d, confirm that the particles are aluminum oxide, as expected. The intensity for aluminum is highest at the particle center, indicating that there may be a higher concentration of aluminum there resulting from incomplete oxidation for these large particles.

EDS spectra from large areas for each sample are presented in Figure 4a, with a smaller scale plot of sample 1 in Figure 4b. Results for the 1.8 nm diameter particles in sample 1 show that there are trace amounts of aluminum present on the substrate after oxidation, likely as molecular aluminum oxide coating the area where the clusters had been deposited. Although the amount of aluminum deposited was nominally the same, the amount of aluminum present on the substrate increases significantly for the larger particle sizes in samples 2 and 3. XPS was performed on duplicate samples on silicon substrates to verify the EDS results and to qualitatively compare the amounts of aluminum present for each sample. The results presented in Figure 4c show that the amount of aluminum was below the level of detection for sample 1, but there is a significant amount of aluminum in the form of an oxide (74–76 eV)^{53,59} for the 7.5 and 8.4 nm diameter particles in samples 2 and 3, respectively. The peak intensity is 7.5× larger for the 8.4 nm diameter particles than the 7.5 nm diameter particles, which agrees well with the 7× increase in particle coverage noted in the ADF-STEM results.

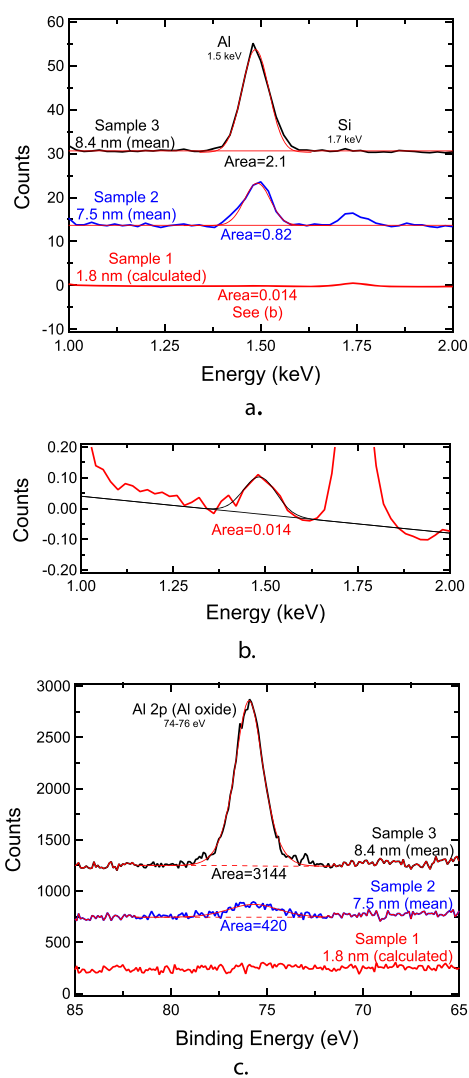


Figure 4. (a) Energy dispersive spectroscopy (EDS) spectra showing the aluminum peaks from each sample, with sample 1 replotted in (b) on a smaller scale to show its aluminum peak which is not visible on the scale of samples 2 and 3. (c) X-ray photoelectron spectroscopy (XPS) data of the same particles. Both analytical techniques agree that there is significantly more aluminum present for sample 3 (8.4 nm in diameter) than sample 2 (7.5 nm in diameter) and that there are only trace amounts of aluminum for sample 1 (1.8 nm in diameter).

IV. DISCUSSION

ADF-STEM micrographs of sample 1 (average particle diameter of 1.8 nm) show that there are no particles on the substrate, despite the fact that in situ quadrupole mass spectroscopy confirms that a significant amount of aluminum was doped into the helium droplets and transition size nanoparticles had formed. These samples were replicated multiple times, and there were never any particles observed by

TEM after removal from a vacuum. Broad EDS scans show that only a trace amount of aluminum oxide remained on the substrates.

ADF-STEM images of sample 2 (average particle diameter ≈ 7.5 nm) show that the particles present on the surface are larger and less numerous than anticipated. The most reasonable explanation for this is that whatever causes the disappearance of the 1.8 nm diameter particles from sample 1 is also occurring at the lower end of the size distribution of particles in sample 2, skewing the measured average toward larger sizes and resulting in a lower coverage than expected. *The smallest particles observed in sample 2 were ≈ 4 nm in diameter, suggesting that this may be the threshold size for particle stability.* The particles from sample 3 (8.4 nm in diameter) were of a size and coverage that agree with calculations after taking multicenter growth into account, indicating minimal loss of aluminum from the surface.⁶⁰

A Comparison of Ejection Mechanisms. The first possible explanation for our findings that larger particles are found on the substrate while smaller particles are not could be that smaller particles simply do not achieve successful deposition. Destruction upon landing is unlikely, however, since our method of deposition is gentle (≈ 0.05 eV/atom), and aluminum particles have been shown to survive more typical soft-landing conditions (0.14 eV/atom) elsewhere.³⁵ It is also unlikely that the smaller particles simply bounce off the substrate while larger particles do not. Experimental work⁶¹ and DFT simulations⁶² agree that rebounding or evaporation does not occur for particles of any size due to the cushioning effect of the helium droplet vaporizing as it contacts the substrate. We also tried to detect bouncing in these experiments as well by placing a residual gas analyzer (RGA) placed at an angle to the substrate during deposition where it could detect material bouncing off the surface. No measurable amount of aluminum was observed with this method. Therefore, we find it highly unlikely that particles of any size are bouncing off the substrate.

Another possible explanation may be that radius-dependent vapor pressure of the particle reaches a threshold such that the smaller particles sublimate while sitting in a vacuum, and the larger particles do not. Simple calculations based on the Kelvin equation, however, show that this is extremely unlikely to occur at room temperature for particles of any size.⁵

It has also been conjectured that aluminum does not form particles in helium droplets, but rather a dissociated foam of atoms, because other groups were unable to achieve significant depletion of the helium beam monitored by mass spectroscopy.⁶³ However, that work was performed with very low doping rates, with up to 8 atoms/droplet, whereas we dope from 200 to 80000 atoms/droplet. It is now clear that aluminum can indeed be incorporated into the droplets at these higher doping rates, as confirmed by the reported beam depletion (50% of He_2^+ peak), mass spectra shown in Figure 2, and images of the resulting particles in Figure 3.

It is more likely that the smaller particles are ejecting the majority of their mass during oxidation. They are not passivated before sudden exposure to ambient air, and based on the vacuum level and partial pressures of oxygen-containing molecules in our system during deposition, the particles can be expected to have at most 1–2 monolayers (< 1 nm) of hydroxylated aluminum on the surface. Therefore, it is feasible that these unpassivated particles just a few nanometers in diameter will spontaneously eject material upon exposure to

air. There seem to be four primary ways that aluminum particles can eject material during oxidation: (1) pressurization within a solid shell which bursts (melt dispersion mechanism),⁶⁴ (2) vapor-phase combustion,²⁹ (3) oxide ejection from the shell during rapid heating,⁶⁵ and (4) oxygen etching.²⁷

According to the melt dispersion mechanism, an oxide shell forms around a combusting aluminum particle early in the reaction. When the internal core melts and expands, pressure is exerted on the shell, causing it to crack. The sudden exposure of fresh molten aluminum leads to a rapid increase in temperature and the subsequent ejection of the molten material, leaving behind a hollow shell.^{30,64} The melt dispersion mechanism is highly unlikely for this scenario because a minimal shell (a single monolayer of oxide) would consume 38% of aluminum deposited, considering the fraction of surface atoms for particles < 4 nm in diameter, and this large fraction of oxide remaining would be detectable by XPS. Furthermore, the shell would likely be too thin to maintain any pressurization⁶⁶ and may even be molten during oxidation due to forming a lower melting point suboxide according to the Cabrera–Mott effect.^{24,67,68}

In vapor-phase combustion, an aluminum particle oxidizes at high enough temperature for a molten particle to evaporate aluminum from the surface and burn as a vapor in a flame surrounding the particle.² This is possible because the adiabatic temperature of aluminum oxidation is higher than the boiling point of aluminum. Vapor-phase oxidation is also very unlikely for this scenario, however, because not only would the particle have to be at a high enough temperature to boil but also vapor-phase oxidation cannot be sustained for particles smaller than a few micrometers. As the particle size decreases below the mean free path of the environment gas molecules, convection of heat from the flame to the particle is insufficient to keep it hot enough to react.⁶⁹ Coupling this with the fact that these transition size nanoparticles are cooling via conduction to the substrate in this particular test as well, it seems unlikely for the particles as a whole to be heating to the extent that they undergo vapor-phase combustion.

One mechanism that can explain the disappearance of particles is the ejection of oxide clusters from the oxide shell. Vashishta et al. have performed computational studies on the oxidation of aluminum nanoparticles with thin alumina shells (total diameter 26–50 nm) that show the ejection of aluminum oxide clusters of varying Al/O ratios.^{65,70–73} Other simulations performed on 4 nm diameter aluminum particles with oxide shells from 0.6 to 1.0 nm thick show that AlO nanoclusters are ejected from the suboxide shell which melts very early in the reaction and at relatively low temperatures.²⁴ The exact mechanism of ejecting oxide clusters from the shell is still unclear, but these results are in agreement with experimental work in which AlO was detected for aluminum nanoparticles under high pressures and heating rates.³⁷ While this behavior has only been validated by experiments under extreme conditions (shock-tube tests), this ejection mechanism may be possible under the conditions in our experiment as well. It could explain our observations if only particles with diameters < 4 nm can oxidize and heat rapidly enough because their increased surface area allows for faster reactions.

The last mechanism of material ejection is oxygen etching, which has previously only been observed with atomic clusters measured in the gas phase.^{15,18,19,28} The reaction between an

oxygen molecule and surface aluminum atom is sufficiently exothermic to eject the reaction product from the material. Under these conditions, the cohesive energy is comparatively low, and the energy released from oxidation cannot be dissipated quickly over the few bonds a surface atom possesses, whereas in our experiments, the particles are larger and sitting on a substrate that can act as a heat sink. Of the four potential mechanisms, this is the only one that does not require the whole particle to be at elevated temperature or at significant pressure and is the only one that can occur during slow oxidation. It can explain our observed results if there is a threshold at 4 nm, below which particles behave as clusters during oxidation and above which they behave like typical nanoparticles (heterogeneous oxidation).

Behavior under Slow Oxidation Conditions. Of the two oxidation mechanisms that could explain the apparent vaporization of particles <4 nm in diameter, one requires rapid heating and high temperatures, while the other can occur very slowly and at low temperatures. We therefore designed an additional experiment to distinguish between them. For this test, we reproduced two more replicates of the 1.8 nm diameter particles from sample 1. One was oxidized rapidly after deposition, and the other was left under vacuum and steadily brought up to ambient pressure by bleeding in oxygen over the course of 44 h—too slowly for particle heating to occur (the collision rate is 12 orders of magnitude lower at the starting vacuum level than in ambient air). The two samples were then imaged by using ADF-STEM, and EDS spectra were collected from large areas. The EDS results, presented in Figure 5, were normalized such that the intensities of their carbon peaks are equal to directly compare all samples. The silicon peak is from a minor impurity from diffusion pump oil contamination of the beam and provides some scale for how small the aluminum peak is. The intensity of the aluminum peaks for slow oxidation (0.027) and fast oxidation (0.038) are greater than that of sample 1 (0.014), shown in Figure 4b, but all of these values correspond to just trace amounts at the lower limits of detection and are insignificant in comparison to samples 2 and 3 for which particles were observed. A comparison of the ADF-STEM images in Figures 3a and 5 supports that all the 1.8 nm diameter samples are nominally the same and do not contain particles regardless of exposure method. This indicates that *rapid oxidation is not necessary for the vaporization of the particles <4 nm in diameter*, and the only reasonable mechanism that applies is oxygen etching.

Critical Diameter. As the particle diameter decreases, the average coordination number (CN) of the system, which is directly related to the cohesive energy (sublimation energy), does not vary significantly until a steep drop-off that starts at ~5 nm.^{74,75} Molecular dynamics simulations^{76,77} and experimental work⁷⁸ have shown that the cohesive energy of aluminum clusters is proportional to cluster size and is smaller than its bulk value of 3.3 eV/atom, but the specific size at which cohesive energy starts to deviate from the bulk is unknown. There are, however, studies that show strong declines in related properties like melting temperature⁷⁹ and vaporization temperature⁸⁰ starting near 5 nm as well, closely mimicking the trend for the underlying parameter, average CN. Shandiz et al.⁷⁴ have developed an equation to estimate the average CN (\bar{Z}_p) of a nanoparticle as a function of diameter (D):

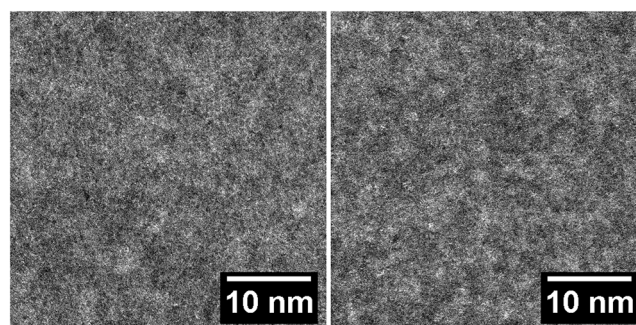
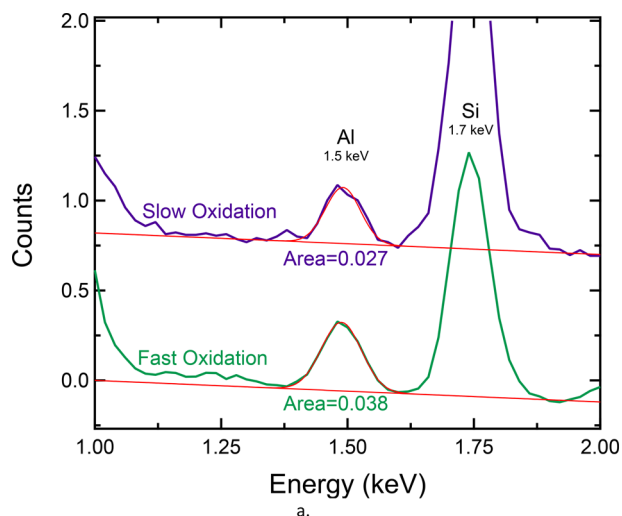


Figure 5. (a) Broad EDS scans showing that there is no significant difference between the 1.8 nm diameter particle samples that are oxidized rapidly or slowly. Both have just trace amounts of aluminum present after exposure. ADF-STEM images of the fast oxidation sample (b) and the slow oxidation sample (c) show that no particles are present regardless of oxidation rate. The results can be compared directly to those presented in Figures 3 and 4.

$$\bar{Z}_p = Z_{Lp} \left(1 - 2(1 - q) \frac{D_0}{D + D_0} \right)$$

where Z_{Lp} is the CN of atoms in the lattice, q is the ratio of CN of atoms on the surface to that of atoms in the lattice, and D_0 is the critical diameter at which all of the atoms are on the surface. Figure 6 is a plot of the above equation calculated for three aluminum FCC crystal surfaces (111), (100), and (110) by using $D_0 = 0.70, 0.61,$ and 0.43 nm, respectively, based on the atomic radius of aluminum and the varying areal densities for each plane. An estimate of $q = 3/8$ was used for each because it is the average of $1/2$ (best for particles >10 nm) and 1 (best for particles <10 nm).⁸⁰ This variability in q arises because it is also a function of D . As the particle diameter decreases, the extent of faceting and therefore the fraction of edges and corners increase, and atoms at these sites have significantly lower CNs than sites on a flat surface. Figure 7 demonstrates how the CN of the surface atoms increase as diameter decreases, which is more relevant to surface atoms vaporizing than the average particle CN is. This calculation was performed for truncated octahedra of FCC gold, which is expected to be very similar to aluminum particles, particularly those with >300 atoms, which also form FCC truncated octahedra.⁸²

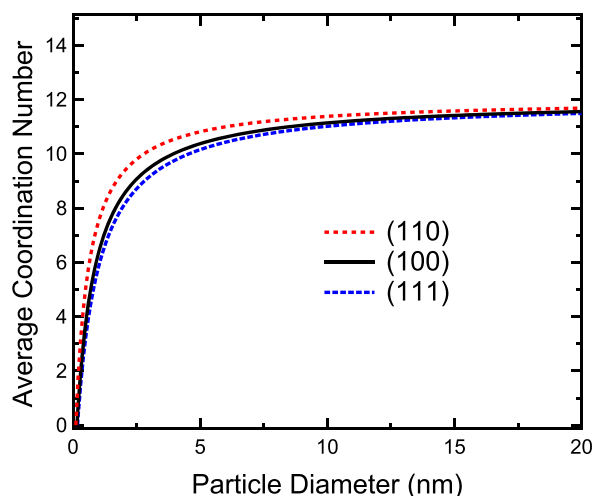


Figure 6. Average coordination number as a function of aluminum particle diameter for particles with (110), (100), and (111) FCC surfaces.

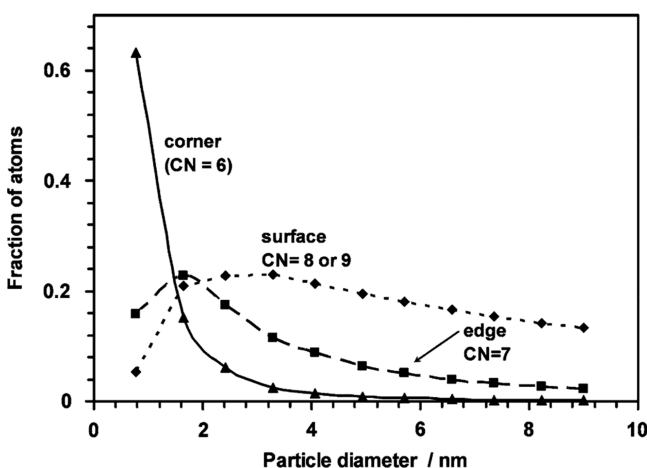


Figure 7. Fraction of atoms located at corner sites, edge sites, or on a surface facet, as a function of particle diameter. Reproduced with permission from ref 81. Copyright 2007 Springer Nature.

It is important to distinguish between atom sites because atoms with a low CN are more accessible to the impinging oxygen molecules and have greater binding energy to that oxygen due to a larger quantity of dangling bonds, making these sites more favorable for reactions.⁸³ This is demonstrated in catalytic work where, for example, CO and oxygen do not adsorb onto gold particle sites with a CN > 7, so the preferred (111) surface orientation (CN = 8–9) is inactive while edges (CN = 7) and corners (CN = 6) are active.⁸¹

Surface atoms on smaller particles may also be more likely to evaporate because the electronic density of states for a particle decreases with diameter. The energy released when an oxygen molecule binds to the surface atoms does not have as many states available to excite in the surrounding atoms, causing that energy to stay localized to the newly formed aluminum oxide molecules. Essentially, smaller particles experience a partial loss of metallic character and therefore have a slight reduction in thermal conductivity compared to larger particles. It has been shown that magnesium particles experience a gradual metal/nonmetal transition around 1 nm,⁸² but it is feasible that aluminum particles could experience a partial loss of metallic

bonding locally at the corners and edges of particles near 4 nm in diameter due to this quantum size effect.

Given the potential for increased reactivity, increased exothermicity, and decreased energy dissipation for particles in this size range, it is feasible that there is a crossover point for aluminum oxidation behavior at a diameter near 4 nm. On a flat aluminum FCC (111) surface, which is the thermodynamically favored surface for particles in this size range,^{77,84} the dissociative adsorption of O₂ has an energy ($\Delta E_{\text{adsorption}}$) of -8.8 eV.⁸⁵ As previously mentioned, interactions with edge and corner atoms may be more energetic. The cohesive energy of a surface atom (E_{cohesive}) is likely close to -2.9 eV/atom, which is the average cohesive energy of a small cluster for which most of the atoms are surface atoms.^{76,77} We propose that the apparent critical diameter of 4 nm may exist because this is the diameter at which

$$E_{\text{cohesive}} = \frac{\Delta E_{\text{adsorption}}}{N}$$

where N is the number of aluminum atoms interacting with the impinging oxygen. For example, the above literature values for similar conditions ($\Delta E_{\text{diss}} = -8.8$ eV and $E_{\text{coh,SA}} = -2.9$ eV/atom) are applicable if the energy of dissociation is predominantly dispersed between three aluminum atoms ($N = 3$ atoms). It is feasible that as the CN of the aluminum particles decreases with particle size, there is a threshold near 4 nm in diameter where such an interaction with three surface atoms becomes more likely than an interaction with four surface atoms. For particles >4 nm, the energy of oxygen adsorption is dissipated into the particle and a solid oxide forms, making future vaporization more difficult. Below this point, the energy of oxygen adsorption can overcome the binding energy of these atoms, and they are ejected from the surface. This transition point could potentially be quite sharp because there is a positive feedback loop: when a solid oxide forms, future vaporization becomes less likely because that surface now has a refractory oxide shell. However, if vaporization occurs, future vaporization becomes more likely since the particle size decreases further, and a fresh surface with an even lower CN is exposed. Of course, the combination of values that satisfy this condition may differ significantly, as it depends upon the crystal structure of each face, number of edges, and so on. If such a threshold exists, though, we would qualitatively expect it to be near this value and occur for particle diameters near 4 nm, based on the underlying trend of decreasing coordination of the surface atoms.

This hypothesis based on the increased activity of edge and corner sites also helps reconcile the apparent contradiction between the oxygen etching of small particles and the common practice of reactive sputtering aluminum in the presence of oxygen to deposit films of alumina (Al₂O₃).⁸⁶ In reactive sputtering, the partial pressure of oxygen is low enough that the mean free path of the aluminum atoms is much greater than the distance to the substrate, and so collisions are not expected until after the aluminum is already on the surface. If small particles of aluminum etch when they interact with oxygen, especially on a heated surface, this technique should not be possible. However, the fundamental principles of thin-film growth dictate that under such conditions, metal films form via the Volmer–Weber mechanism in which the highly mobile aluminum adatoms deposited onto the surface coalesce and form islands with large radii of curvature, and will eventually grow in size until the islands come in contact and

form a film.⁸⁷ The radius of curvature for such an island would be much greater than a spherical particle of the same mass sitting on the surface and would therefore have far fewer corners and edges. These islands would therefore be expected to oxidize normally and not be etched away.

The importance of radius of curvature is also apparent when comparing these results against the low-temperature oxidation of thin films of aluminum performed in vacuum with low concentrations of oxygen. These studies show that amorphous, Al-deficient (compared to Al_2O_3) films form very rapidly (<250 s) with a limiting thickness of ~ 0.7 nm, depending on the temperature, oxygen concentration, and packing density of the crystal face.^{38,88} Despite very similar conditions, oxygen etching is not observed because the aluminum is a flat crystalline surface rather than small particles.

Further Evidence from Aluminum/Gold Composite Particles. We have performed additional experiments to test our hypothesis that small aluminum particles undergo oxygen etching based predominantly upon the radius of curvature of the particle. This was accomplished by using SHeDA to produce inert gold particles coated with shells of aluminum. Additional details about the aluminum/gold composite materials can be found elsewhere.⁸⁹ The first set of Al/Au composite particles were core-shell particles with ≈ 5 nm gold cores and ≈ 1 nm aluminum shells. In this configuration, the relevant length scale for the aluminum is even smaller than the smallest aluminum particles from previous samples, but the radius of curvature is much larger because it is on the outside of a large, inert particle. The ADF-STEM image in Figure 8a

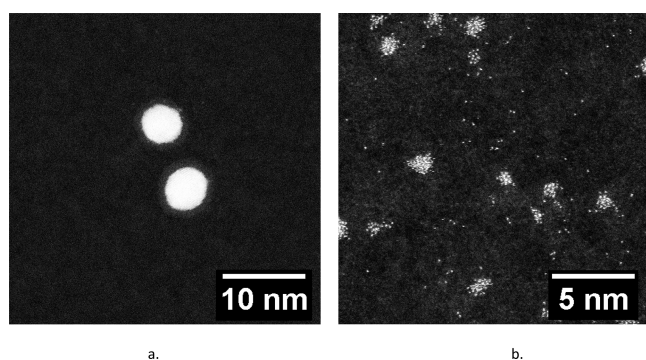


Figure 8. ADF-STEM images of aluminum/gold composite particles. (a) Particles with 1 nm aluminum shells on 5 nm diameter gold cores. The aluminum remains on the surface, indicating that it does not etch when in a configuration with a large radius of curvature. (b) Similar particles but with a smaller gold core only 1 nm in diameter to decrease the radius of curvature of the aluminum surface. Aluminum is ejected from the substrate upon exposure to air, leaving small gold clusters and stray atoms on the substrate.

shows that after exposure to air there is an intact alumina shell remaining on the particles. A second set of composite particles were produced that were similar to the first (1 nm aluminum shells around inert gold cores), except the gold cores for these samples were only 1 nm in diameter. Therefore, the primary difference between the samples was that the radius of curvature of the aluminum surface was much smaller for the second sample. The ADF-STEM image in Figure 8b shows that after exposure to air the substrate was covered with bare gold particles ~ 1 nm in diameter, and there were trace amounts of aluminum oxide dispersed across the surface.

The result that the oxygen etching reaction does not occur for the first sample (large radius of curvature) but does for the second sample (small radius of curvature) supports our proposed explanation that the threshold is dominated by the radius of curvature, which dictates the coordination number of the surface atoms. The result that gold particles remain on the surface for the smaller core/shell particles also supports that particles <4 nm in diameter are indeed being successfully deposited and were not simply bouncing off the substrate.

Future Work. We are working toward in-situ XPS experiments to observe the surface immediately after deposition onto a temperature-controlled substrate. We plan to monitor the particles as they are exposed to low partial pressures of oxygen to determine how the surface changes as a function of exposure time and temperature. This is not yet possible due to instrumental restrictions and the inability to maintain UHV during transfer to an external XPS system. We also plan to perform in-situ nanocalorimetry to measure the energetic responses at various heating rates. Both of these tests can be performed on a range of particle sizes, morphologies, and core/shell composite systems using superfluid helium droplet assembly (SHeDA).

V. CONCLUSIONS

Aluminum particles of diameters ranging from 1 to 10 nm were formed by using SHeDA and subsequently oxidized by rapidly transferring the samples from ultrahigh vacuum to ambient air. The samples were then analyzed by using ADF-STEM/EDS and XPS. We found that particles <4 nm in diameter had vaporized during oxidation, while particles >4 nm in diameter remained on the substrate as aluminum oxide. The oxygen-etching mechanism was determined to be the most likely explanation for the vaporization of the smallest particles because it occurs under vacuum conditions with trace oxygen levels, in which significant particle heating was not feasible.

It has been known for decades that upon interacting with oxygen, atomic clusters of aluminum are etched while aluminum nanoparticles undergo heterogeneous oxidation. It follows that there must be a size at which a transition occurs between the two oxidation mechanisms. On the basis of our observations, it seems that the transition occurs near a diameter of 4 nm, likely due to a decrease in coordination number around this size.

■ AUTHOR INFORMATION

Corresponding Author

*E-mail kyle.overdeep.ctr@us.af.mil.

ORCID

Kyle R. Overdeep: 0000-0001-5398-0346

Scott L. Anderson: 0000-0001-9985-8178

Notes

The authors declare no competing financial interest.

■ ACKNOWLEDGMENTS

The efforts conducted at Eglin Air Force Base were supported by the Air Force Office of Scientific Research under AFOSR Award No. 17RWCOR451. ADF-STEM work was performed at the National High Magnetic Field Laboratory of Florida State University, which is supported by the National Science Foundation Cooperative Agreement No. DMR-1157490 and DMR-1644779, and the State of Florida. XPS was performed at the University of Utah in the Micrometer Microscopy Suite

sponsored by the College of Engineering, Health Sciences Center, Office of the Vice President for Research, and the Utah Science Technology and Research (USTAR) initiative of the State of Utah. Work at the University of Utah was supported by the Office of Naval Research under Grant N00014-15-1-2681.

■ ADDITIONAL NOTE

“All particle sizes of relevance here are technically “nanoparticles”, and so for clarity we shall refer to any particles <1 nm in diameter as “clusters”, particles from 1 to 10 nm as “transition size nanoparticles”, and particles from 10 to 1000 nm simply as “nanoparticles”. The term “particle” will be used for general materials of no specific size or materials spanning multiple size ranges.

■ REFERENCES

- (1) Zachariah, M. R.; Egan, G. C. *Mechanisms and Microphysics of Energy Release Pathways in Nanoenergetic Materials*; Elsevier Inc.: 2016.
- (2) Sundaram, D. S.; Puri, P.; Yang, V. A General Theory of Ignition and Combustion of Nano- and Micron-Sized Aluminum Particles. *Combust. Flame* **2016**, *169*, 94–109.
- (3) Dreizin, E. L. Metal-Based Reactive Nanomaterials. *Prog. Energy Combust. Sci.* **2009**, *35*, 141–167.
- (4) Huang, Y.; Risha, G. A.; Yang, V.; Yetter, R. A. Effect of Particle Size on Combustion of Aluminum Particle Dust in Air. *Combust. Flame* **2009**, *156*, 5–13.
- (5) Rai, A.; Park, K.; Zhou, L.; Zachariah, M. R. Understanding the Mechanism of Aluminium Nanoparticle Oxidation. *Combust. Theory Modell.* **2006**, *10*, 843–859.
- (6) Ermoline, A.; Dreizin, E. L. Equations for the Cabrera – Mott Kinetics of Oxidation for Spherical Nanoparticles. *Chem. Phys. Lett.* **2011**, *505*, 47–50.
- (7) Dreizin, E. L.; Schoenitz, M. Correlating Ignition Mechanisms of Aluminum-Based Reactive Materials with Thermoanalytical Measurements. *Prog. Energy Combust. Sci.* **2015**, *50*, 81–105.
- (8) Sundaram, D. S.; Yang, V.; Zarko, V. E. Combustion of Nano Aluminum Particles (Review). *Combust., Explos. Shock Waves* **2015**, *51*, 173–196.
- (9) Coulet, M.-V.; Rufino, B.; Esposito, P.-H.; Neisius, T.; Isnard, O.; Denoyel, R. Oxidation Mechanism of Aluminum Nanopowders. *J. Phys. Chem. C* **2015**, *119*, 25063–25070.
- (10) Campbell, T.; Kalia, R. K.; Nakano, A.; Vashishta, P.; Ogata, S.; Rodgers, S. Dynamics of Oxidation of Aluminum Nanoclusters Using Variable Charge Molecular-Dynamics Simulations on Parallel Computers. *Phys. Rev. Lett.* **1999**, *82*, 4866–4869.
- (11) Campbell, T. J.; Aral, G.; Ogata, S.; Kalia, R. K.; Nakano, A.; Vashishta, P. Oxidation of Aluminum Nanoclusters. *Phys. Rev. B: Condens. Matter Mater. Phys.* **2005**, *71*, 205413.
- (12) Woodward, W. H.; Eyet, N.; Shuman, N. S.; Smith, J. C.; Viggiano, A. A.; Castleman, A. W. Aluminum Cluster Anion Reactivity with Singlet Oxygen: Evidence of Al₉- Stability. *J. Phys. Chem. C* **2011**, *115*, 9903–9908.
- (13) Leuchtner, R. E.; Harms, A. C.; Castleman, A. W. Thermal Metal Cluster Anion Reactions: Behavior of Aluminum Clusters with Oxygen. *J. Chem. Phys.* **1989**, *91*, 2753–2754.
- (14) Leuchtner, R. E.; Harms, A. C.; Castleman, A. W. Aluminum Cluster Reactions. *J. Chem. Phys.* **1991**, *94*, 1093–1101.
- (15) Cooper, B. T.; Parent, D.; Buckner, S. W. Oxidation Reactions and Photochemistry of Aluminum Cluster Anions (Al₃- to Al₂₃-). *Chem. Phys. Lett.* **1998**, *284*, 401–406.
- (16) Reber, A. C.; Khanna, S. N.; Roach, P. J.; Woodward, W. H.; Castleman, A. W. Spin Accommodation and Reactivity of Aluminum Based Clusters with O₂. *J. Am. Chem. Soc.* **2007**, *129*, 16098–16101.
- (17) Luo, Z.; Castleman, A. W.; Khanna, S. N. Reactivity of Metal Clusters. *Chem. Rev.* **2016**, *116*, 14456–14492.
- (18) Fuke, K.; Nonose, S.; Kikuchi, N.; Kaya, K. Reaction of Aluminum Clusters, Al_n (N = 7–24), with Oxygen and Ammonia. *Chem. Phys. Lett.* **1988**, *147*, 479–483.
- (19) Jarrold, M. F.; Bower, J. E. The Reactions of Mass Selected Aluminum Cluster Ions, Al_n (N = 4–25), with Oxygen. *J. Chem. Phys.* **1986**, *85*, 5373.
- (20) Jarrold, M. F.; Bower, J. E. A Detailed Study of the Reactions between Size Selected Aluminum Cluster Ions, Al_n (N = 3–26), and Oxygen. *J. Chem. Phys.* **1987**, *87*, 5728.
- (21) Cox, D. M.; Trevor, D. J.; Whetten, R. L.; Kaldor, A. Aluminum Clusters: Ionization Thresholds and Reactivity toward Deuterium, Water, Oxygen, Methanol, Methane, and Carbon Monoxide. *J. Phys. Chem.* **1988**, *92*, 421–429.
- (22) Hong, S.; van Duin, A. C. T. Molecular Dynamics Simulations of the Oxidation of Aluminum Nanoparticles Using the ReaxFF Reactive Force Field. *J. Phys. Chem. C* **2015**, *119*, 17876–17886.
- (23) Chu, Q.; Shi, B.; Liao, L.; Luo, K. H.; Wang, N.; Huang, C. Ignition and Oxidation of Core – Shell Al/Al₂O₃ Nanoparticles in an Oxygen Atmosphere: Insights from Molecular Dynamics Simulation. *J. Phys. Chem. C* **2018**, *122*, 29620–29627.
- (24) Zeng, H.; Cheng, X.; Zhang, C.; Lu, Z. Responses of Core–Shell Al/Al₂O₃ Nanoparticles to Heating: ReaxFF Molecular Dynamics Simulations. *J. Phys. Chem. C* **2018**, *122*, 9191–9197.
- (25) Henz, B. J.; Hawa, T.; Zachariah, M. R. Atomistic Simulation Of The Aluminum Nanoparticle Oxidation Mechanism. In *48th AIAA Aerospace Sciences Meeting Including the New Horizons Forum and Aerospace Exposition*; 2010; pp 1–9.
- (26) Chung, S. W.; Gulians, E. A.; Bunker, C. E.; Jelliss, P. A.; Buckner, S. W. Size-Dependent Nanoparticle Reaction Enthalpy: Oxidation of Aluminum Nanoparticles. *J. Phys. Chem. Solids* **2011**, *72*, 719–724.
- (27) Neumaier, M.; Olzmann, M.; Kiran, B.; Bowen, K. H.; Eichhorn, B.; Stokes, S. T.; Buonaugurio, A.; Burgert, R.; Schnöckel, H. The Reaction Rates of O₂ with Closed-Shell and Open-Shell Al_x- and Ga_x- Clusters under Single-Collision Conditions: Experimental and Theoretical Investigations toward a Generally Valid Model for the Hindered Reactions of O₂ with Metal Atom Clusters. *J. Am. Chem. Soc.* **2014**, *136*, 3607–3616.
- (28) Armentrout, P. B. Reactions and Thermochemistry of Small Transition Metal Cluster Ions. *Annu. Rev. Phys. Chem.* **2001**, *52*, 423–461.
- (29) Ermoline, A.; Yildiz, D.; Dreizin, E. L. Model of Heterogeneous Combustion of Small Particles. *Combust. Flame* **2013**, *160*, 2982–2989.
- (30) Levitas, V. I.; Asay, B. W.; Son, S. F.; Pantoya, M. Melt Dispersion Mechanism for Fast Reaction of Nanothermites. *Appl. Phys. Lett.* **2006**, *89*, 071909.
- (31) Maurice, V.; Marcus, P. STM Study of Sputter-Deposited Al Clusters in Chemical Interaction with Graphite (0001) Surfaces. *Surf. Sci.* **1992**, *275*, 65–74.
- (32) Hinnen, C.; Imbert, D.; Siffre, J.M.; Marcus, P. An in Situ XPS Study of Sputter-Deposited Aluminium Thin Films on Graphite. *Appl. Surf. Sci.* **1994**, *78*, 219–231.
- (33) Woodward, W. H.; Blake, M. M.; Luo, Z.; Weiss, P. S.; Castleman, A. W. Soft-Landing Deposition of Al₁₇- on a Hydroxyl-Terminated Self-Assembled Monolayer. *J. Phys. Chem. C* **2011**, *115*, 5373–5377.
- (34) Lai, S. L.; Carlsson, J. R. A.; Allen, L. H. Melting Point Depression of Al Clusters Generated during the Early Stages of Film Growth: Nanocalorimetry Measurements. *Appl. Phys. Lett.* **1998**, *72*, 1098–1100.
- (35) Klipp, B.; Grass, M.; Müller, J.; Stolcic, D.; Lutz, U.; Ganteför, G.; Schlenker, T.; Boneberg, J.; Leiderer, P. Deposition of Mass-Selected Cluster Ions Using a Pulsed Arc Cluster-Ion Source. *Appl. Phys. A: Mater. Sci. Process.* **2001**, *73*, 547–554.
- (36) Bazyn, T.; Krier, H.; Glumac, N. Combustion of Nanoaluminum at Elevated Pressure and Temperature behind Reflected Shock Waves. *Combust. Flame* **2006**, *145*, 703–713.

- (37) Lynch, P.; Fiore, G.; Krier, H.; Glumac, N. Gas-Phase Reaction in Nanoaluminum Combustion. *Combust. Sci. Technol.* **2010**, *182*, 842–857.
- (38) Jeurgens, L. P. H.; Sloof, W. G.; Tichelaar, F. D.; Mittemeijer, E. J. Growth Kinetics and Mechanisms of Aluminum-Oxide Films Formed by Thermal Oxidation of Aluminum. *J. Appl. Phys.* **2002**, *92*, 1649.
- (39) Toennies, J. P.; Vilesov, A. F. Superfluid Helium Droplets: A Uniquely Cold Nanomatrix for Molecules and Molecular Complexes. *Angew. Chem., Int. Ed.* **2004**, *43*, 2622–2648.
- (40) Emery, S. B.; Xin, Y.; Ridge, C. J.; Buszek, R. J.; Boatz, J. A.; Boyle, J. M.; Little, B. K.; Lindsay, C. M. Unusual Behavior in Magnesium-Copper Cluster Matter Produced by Helium Droplet Mediated Deposition. *J. Chem. Phys.* **2015**, *142*, 084307.
- (41) Emery, S. B.; Rider, K. B.; Lindsay, C. M. Stabilized Magnesium/Perfluoropolyether Nanocomposite Films by Helium Droplet Cluster Assembly. *Propellants, Explos., Pyrotech.* **2014**, *39*, 161–165.
- (42) Haberfehlner, G.; Thaler, P.; Knez, D.; Volk, A.; Hofer, F.; Ernst, W. E.; Kothleitner, G. Formation of Bimetallic Clusters in Superfluid Helium Nanodroplets Analysed by Atomic Resolution Electron Tomography. *Nat. Commun.* **2015**, *6*, 8779.
- (43) Loginov, E.; Gomez, L. F.; Sartakov, B. G.; Vilesov, A. F. Formation of Large Ag Clusters with Shells of Methane, Ethylene, and Acetylene in He Droplets. *J. Phys. Chem. A* **2016**, *120*, 6738–6744.
- (44) Jeffs, J.; Besley, N. A.; Stace, A. J.; Sarma, G.; Cunningham, E. M.; Boatwright, A.; Yang, S.; Ellis, A. M. Metastable Aluminum Atoms Floating on the Surface of Helium Nanodroplets. *Phys. Rev. Lett.* **2015**, *114*, 233401.
- (45) Harruff-Miller, B. A.; Bunker, C. E.; Lewis, W. K. Infrared Spectroscopy of the N₃ Band of C₃ in Helium Droplets. *AIP Adv.* **2018**, *8*, 025308.
- (46) Franke, P. R.; Douberly, G. E. Rotamers of Isoprene: Infrared Spectroscopy in Helium Droplets and Ab Initio Thermochemistry. *J. Phys. Chem. A* **2018**, *122*, 148–158.
- (47) Cleaver, R. M.; Lindsay, C. M. Detailed Design and Transport Properties of a Helium Droplet Nozzle from 5 to 50 K. *Cryogenics* **2012**, *52*, 389–397.
- (48) Gomez, L. F.; Loginov, E.; Sliter, R.; Vilesov, A. F. Sizes of Large He Droplets. *J. Chem. Phys.* **2011**, *135*, 154201.
- (49) Loginov, E.; Gomez, L. F.; Vilesov, A. F. Surface Deposition and Imaging of Large Ag Clusters Formed in He Droplets. *J. Phys. Chem. A* **2011**, *115*, 7199–7204.
- (50) Thaler, P.; Volk, A.; Ratschek, M.; Koch, M.; Ernst, W. E. Molecular Dynamics Simulation of the Deposition Process of Cold Ag-Clusters under Different Landing Conditions. *J. Chem. Phys.* **2014**, *140*, 044326.
- (51) Cueva, P.; Hovden, R.; Mundy, J. A.; Xin, H. L.; Muller, D. A. Data Processing for Atomic Resolution Electron Energy Loss Spectroscopy. *Microsc. Microanal.* **2012**, *18*, 667–675.
- (52) Schindelin, J.; Arganda-Carreras, I.; Frise, E.; Kaynig, V.; Longair, M.; Pietzsch, T.; Preibisch, S.; Rueden, C.; Saalfeld, S.; Schmid, B.; et al. Fiji: An Open-Source Platform for Biological-Image Analysis. *Nat. Methods* **2012**, *9*, 676–682.
- (53) Moulder, J. F.; Stickle, W. F.; Sobol, P. E.; Bomben, K. D. In *Handbook of X-Ray Photoelectron Spectroscopy: A Reference Book of Standard Spectra for Identification and Interpretation of XPS Data*; Chastain, J., Ed.; Physical Electronics Division, Perkin-Elmer Corporation: Eden Prairie, MN, 1992.
- (54) Tiggesbäumker, J.; Stienkemeier, F. Formation and Properties of Metal Clusters Isolated in Helium Droplets. *Phys. Chem. Chem. Phys.* **2007**, *9*, 4748–4770.
- (55) Buchenau, H.; Knuth, E. L.; Northby, J.; Toennies, J. P.; Winkler, C. Mass Spectra and Time-of-Flight Distributions of Helium Cluster Beams. *J. Chem. Phys.* **1990**, *92*, 6875.
- (56) Volk, A.; Thaler, P.; Knez, D.; Hauser, A. W.; Steurer, J.; Grogger, W.; Hofer, F.; Ernst, W. E. The Impact of Doping Rates on the Morphologies of Silver and Gold Nanowires Grown in Helium Nanodroplets. *Phys. Chem. Chem. Phys.* **2016**, *18*, 1451–1459.
- (57) Gomez, L. F.; Loginov, E.; Vilesov, A. F. Traces of Vortices in Superfluid Helium Droplets. *Phys. Rev. Lett.* **2012**, *108*, 155302.
- (58) Gomez, L. F.; Ferguson, K. R.; Cryan, J. P.; Bacellar, C.; Tanyag, R. M. P.; Jones, C.; Schorb, S.; Anielski, D.; Belkacem, A.; Bernardo, C.; Boll, R.; Bozek, J.; Carron, S.; Chen, G.; Delmas, T.; Englert, L.; Epp, S. W.; Erk, B.; Foucar, L.; Hartmann, R.; Hexemer, A.; Huth, M.; Kwok, J.; Leone, S. R.; Ma, J. H. S.; Maia, F. R. N. C.; Malmerberg, E.; Marchesini, S.; Neumark, D. M.; Poon, B.; Prell, J.; Rolles, D.; Rudek, B.; Rudenko, A.; Seifrid, M.; Siefertmann, K. R.; Sturm, F. P.; Swiggers, M.; Ullrich, J.; Weise, F.; Zwart, P.; Bostedt, C.; Gessner, O.; Vilesov, A. F. Shapes and Vorticities of Superfluid Helium Nanodroplets. *Science* **2014**, *345*, 906–909.
- (59) Naumkin, A. V.; Kraut-Vass, A.; Gaarenstroom, S. W.; Powell, C. J. NIST X-Ray Photoelectron Spectroscopy Database. *NIST Standard Reference Database 20*; National Institute of Standards and Technology: Gaithersburg, MD, 2012.
- (60) Ridge, C. J.; Wu, Q.; Orlov, A.; Lindsay, C. M. Gold Nanocluster Film Growth by Helium Nanodroplet Deposition. Manuscript in preparation, 2019.
- (61) Wu, Q.; Ridge, C. J.; Zhao, S.; Zakharov, D.; Cen, J.; Tong, X.; Connors, E.; Su, D.; Stach, E. A.; Lindsay, C. M.; et al. Development of a New Generation of Stable, Tunable, and Catalytically Active Nanoparticles Produced by the Helium Nanodroplet Deposition Method. *J. Phys. Chem. Lett.* **2016**, *7*, 2910–2914.
- (62) de Lara-Castells, M. P.; Aguirre, N. F.; Stoll, H.; Mitrushchenkov, A. O.; Mateo, D.; Pi, M. Communication: Unraveling the 4He Droplet-Mediated Soft-Landing from Ab-Initio-Assisted and Time-Resolved Density Functional Simulations: Au@4He300/TiO₂(110). *J. Chem. Phys.* **2015**, *142*, 131101.
- (63) Krasnokutski, S. A.; Huisken, F. Low-Temperature Chemistry in Helium Droplets: Reactions of Aluminum Atoms with O₂ and H₂O. *J. Phys. Chem. A* **2011**, *115*, 7120–7126.
- (64) Levitas, V. I.; Pantoya, M. L.; Dean, S. Melt Dispersion Mechanism for Fast Reaction of Aluminum Nano- and Micron-Scale Particles: Flame Propagation and SEM Studies. *Combust. Flame* **2014**, *161*, 1668–1677.
- (65) Li, Y.; Kalia, R. K.; Nakano, A.; Vashishta, P. Size Effect on the Oxidation of Aluminum Nanoparticle: Multimillion-Atom Reactive Molecular Dynamics Simulations. *J. Appl. Phys.* **2013**, *114*, 134312.
- (66) Litrico, G.; Proulx, P.; Gouriet, J. B.; Rambaud, P. Controlled Oxidation of Aluminum Nanoparticles. *Adv. Powder Technol.* **2015**, *26*, 1–7.
- (67) Chakraborty, P.; Zachariah, M. R. Do Nanoenergetic Particles Remain Nano-Sized during Combustion? *Combust. Flame* **2014**, *161*, 1408–1416.
- (68) Cabrera, N.; Mott, N. F. Theory of the Oxidation of Metals. *Rep. Prog. Phys.* **1949**, *12*, 163.
- (69) Mohan, S.; Trunov, M. A.; Dreizin, E. L. On Possibility of Vapor-Phase Combustion for Fine Aluminum Particles. *Combust. Flame* **2009**, *156*, 2213–2216.
- (70) Wang, W.; Clark, R.; Nakano, A.; Kalia, R. K.; Vashishta, P. Fast Reaction Mechanism of a Core(Al)-Shell(Al₂O₃) Nanoparticle in Oxygen. *Appl. Phys. Lett.* **2009**, *95*, 261901.
- (71) Wang, W.; Clark, R.; Nakano, A.; Kalia, R. K.; Vashishta, P. Effects of Oxide-Shell Structures on the Dynamics of Oxidation of Al Nanoparticles. *Appl. Phys. Lett.* **2010**, *96*, 181906.
- (72) Li, Y.; Clark, R.; Nakano, A.; Kalia, R. K.; Vashishta, P. Molecular Dynamics Study of Size Dependence of Combustion of Aluminum Nanoparticles. *Mater. Res. Soc. Symp. Proc.* **2012**, DOI: 10.1557/opl.2012.346.
- (73) Clark, R.; Wang, W.; Nomura, K.; Kalia, R. K.; Nakano, A.; Vashishta, P. Heat-Initiated Oxidation of an Aluminum Nanoparticle. *Mater. Res. Soc. Symp. Proc.* **2012**, DOI: 10.1557/opl.2012.62.
- (74) Attarian Shandiz, M.; Safaei, A.; Sanjabi, S.; Barber, Z. H. Modeling the Cohesive Energy and Melting Point of Nanoparticles by Their Average Coordination Number. *Solid State Commun.* **2008**, *145*, 432–437.

(75) Li, X. Modeling the Size- and Shape-Dependent Cohesive Energy of Nanomaterials and Its Applications in Heterogeneous Systems. *Nanotechnology* **2014**, *25*, 185702.

(76) Alavi, S.; Thompson, D. L. Molecular Dynamics Simulations of the Melting of Aluminum Nanoparticles. *J. Phys. Chem. A* **2006**, *110*, 1518–1523.

(77) Ojwang', J. G. O.; van Santen, R.; Kramer, G. J.; van Duin, A. C. T.; Goddard, W. A. Predictions of Melting, Crystallization, and Local Atomic Arrangements of Aluminum Clusters Using a Reactive Force Field. *J. Chem. Phys.* **2008**, *129*, 244506.

(78) Starace, A. K.; Neal, C. M.; Cao, B.; Jarrold, M. F.; Aguado, A.; López, J. M. Correlation between the Latent Heats and Cohesive Energies of Metal Clusters. *J. Chem. Phys.* **2008**, *129*, 144702.

(79) Mathur, N.; Mane, T.; Sundaram, D. Atomistically Informed Melting Models for Aluminum Nanocrystals. *Chem. Phys.* **2019**, *522*, 188–198.

(80) Shandiz, M. A. Effective Coordination Number Model for the Size Dependency of Physical Properties of Nanocrystals. *J. Phys.: Condens. Matter* **2008**, *20*, 325237.

(81) Janssens, T. V. W.; Clausen, B. S.; Hvolbæk, B.; Falsig, H.; Christensen, C. H.; Bligaard, T.; Nørskov, J. K. Insights into the Reactivity of Supported Au Nanoparticles: Combining Theory and Experiments. *Top. Catal.* **2007**, *44*, 15–26.

(82) Li, Z. H.; Truhlar, D. G. Nanothermodynamics of Metal Nanoparticles. *Chem. Sci.* **2014**, *5*, 2605–2624.

(83) Roldan Cuenya, B.; Behafarid, F. Nanocatalysis: Size- and Shape-Dependent Chemisorption and Catalytic Reactivity. *Surf. Sci. Rep.* **2015**, *70*, 135–187.

(84) Zhang, W.; Lu, W.-C.; Zang, Q.-J.; Wang, C. Z.; Ho, K. M. Bulklike Structures for Medium-Sized Al_n (N = 31–40) Clusters. *J. Chem. Phys.* **2009**, *130*, 144701.

(85) Lousada, M.; Korzhavyi, P. A. Oxygen Adsorption onto Pure and Doped Al Surfaces – the Role of Surface Dopants. *Phys. Chem. Chem. Phys.* **2015**, *17*, 1667–1679.

(86) Li, Q.; Yu, Y.; Bhatia, C. S.; Marks, L. D.; Lee, S. C.; Chung, Y. W. Low-Temperature Magnetron Sputter-Deposition, Hardness, and Electrical Resistivity of Amorphous and Crystalline Alumina Thin Films. *J. Vac. Sci. Technol., A* **2000**, *18*, 2333.

(87) Kaiser, N. Review of the Fundamentals of Thin-Film Growth. *Appl. Opt.* **2002**, *41* (16), 3053–3060.

(88) Reichel, F.; Jeurgens, L. P. H.; Richter, G.; Mittemeijer, E. J. Amorphous versus Crystalline State for Ultrathin Al₂O₃ Overgrowths on Al Substrates. *J. Appl. Phys.* **2008**, *103*, 093515.

(89) Buszek, R. J.; Overdeep, K. R.; Ridge, C. J.; Lindsay, C. M.; Boatz, J. A. A Theoretical Study of Al/Au Core-Shell Nanocluster Formation. Manuscript in preparation, 2019.